Article

New Selective Haloform-type Reaction Yielding 3-Hydroxy-2,2-difluoroacids: Theoretical Study of the Mechanism

Santiago Olivella, Albert Sol, scar Jimnez, M. Pilar Bosch, and Angel Guerrero

J. Am. Chem. Soc., **2005**, 127 (8), 2620-2627• DOI: 10.1021/ja043522d • Publication Date (Web): 04 February 2005

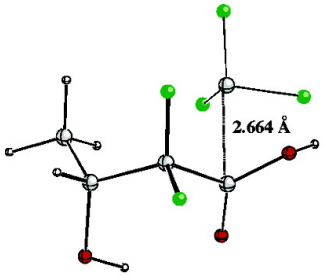

$\Delta G^{\ddagger}(298K)$ = 20.8 kcal/mol

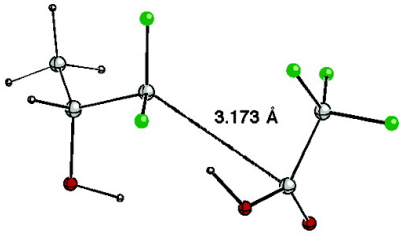

$\Delta G^{\ddagger}(298K)$ = 29.2 kcal/mol

More About This Article

Additional resources and features associated with this article are available within the HTML version:

- Supporting Information
- Links to the 1 articles that cite this article, as of the time of this article download
- Access to high resolution figures
- Links to articles and content related to this article
- Copyright permission to reproduce figures and/or text from this article

View the Full Text HTML

J|A|C|S
ARTICLES
Published on Web 02/04/2005

New Selective Haloform-type Reaction Yielding 3-Hydroxy-2,2-difluoroacids: Theoretical Study of the Mechanism

Santiago Olivella,*,† Albert Solé,‡ Óscar Jiménez,† M. Pilar Bosch,† and Angel Guerrero†

Contribution from the Departament de Quîmica Orgànica Biològica, Institut d'Investigacions Químiques i Ambientals de Barcelona, CSIC, Jordi Girona 18, 08034-Barcelona, Catalonia, Spain and Centre Especial de Recerca en Química Teòrica i Departament de Química Física, Universitat de Barcelona, Martí i Franquès 1, 08028-Barcelona, Catalonia, Spain

Received October 26, 2004; E-mail: sonqtc@cid.csic.es

Abstract: Experimental results of an unprecedented haloform-type reaction in which 4-alkyl-4-hydroxy-3,3-difluoromethyl trifluoromethyl ketones undergo base-promoted selective cleavage of the CO−CF_3 bond, yielding 3-hydroxy-2,2-difluoroacids and fluoroform, are rationalized using DFT (B3LYP) calculations. The gas-phase addition of hydroxide ion to 1,1,1,3,3-pentafluoro-4-hydroxypentan-2-one (**R**) is found to be a barrierless process, yielding a tetrahedral intermediate (**INT**), involving a ΔG_r(298 K) of −61.4 kcal/mol. The CO−CF_3 bond cleavage in **INT** leads to a hydrogen-bonded $[CH_3CHOHCF_2CO_2H\cdots CF_3]^-$ complex by passage through a transition structure (**TS1**) with a $\Delta G^{\ddagger}$(298 K) of 20.8 kcal/mol and a ΔG_r(298 K) of 9.8 kcal/mol. This complex undergoes a proton transfer between its components, yielding a hydrogen-bonded $[CH_3CHOHCF_2CO_2\cdots CHF_3]^-$ complex. This process has associated with it a $\Delta G^{\ddagger}$(298 K) of only 3.1 kcal/mol and a ΔG_r(298 K) of −43.3 kcal/mol. The CO−CF_2 bond cleavage in **INT** leads to a hydrogen-bonded $[CH_3CHOHCF_2\cdots CF_3CO_2H]^-$ complex by passage through a transition structure (**TS3**) with a $\Delta G^{\ddagger}$(298 K) of 29.2 kcal/mol and a ΔG_r(298 K) of 25.1 kcal/mol. The lower energy barrier found for CO−CF_3 bond cleavage in **INT** is ascribed to the larger number of fluorine atoms stabilizing the negative charge accumulated on the CF_3 moiety of **TS1**, as compared to the number of fluorine atoms stabilizing the negative charge on the $CH_3CHOHCF_2$ moiety of **TS3**. The solvent-induced effects on the two pathways, introduced within the SCRF formalism through PCM calculations, do not reverse the predicted preference of the CO−CF_3 over the CO−CF_2 bond cleavage of **R** in the gas phase.

Introduction

It is known that introduction of fluorine atoms into specific positions of organic molecules may cause significant changes in the stability, lipophilicity, and biological activities of the resulting molecules.[1] This has been attributed to the high electronegativity of the halogen, the strong C−F bond, and the similar size of the halogen and hydrogen atoms.[2] For these reasons great effort has been placed on the development and evaluation of biologically active fluorinated materials,[3] particularly in the field of enzymatic inhibition.[4] Inhibition studies carried out with these fluorinated derivatives may be therapeutically important in different areas, e.g., inhibitors of arachidonoyl ethanolamide (anandamide) in processes involving analgesia, mood, nausea, memory, etc.,[5] and renin or angiotensin-converting enzyme inhibitors in hypertension phenomena.[6]

In the course of a work aimed at inhibiting the chemical communication system in insects, a variety of trifluoromethyl ketones,[7] difluoromethyl ketones, and difluoroaldehydes[8] have

† Institut d'Investigacions Químiques i Ambientals de Barcelona, CSIC.
‡ Universitat de Barcelona.

(1) Seebach, D. *Angew. Chem., Int. Ed. Engl.* **1990**, *29*, 1320.
(2) (a) Banks, R. E.; Smart, B. E.; Tatlow, J. C. *Organofluorine Chemistry: Principles and Commercial Applications*; Plenum Press: New York, 1994. (b) Filler, R.; Kobayashi, Y.; Yagupolskii, L. M. *Organofluorine Compounds in Medicinal Chemistry and Biomedical Applications*; Elsevier Science Pub.: Amsterdam, 1993.
(3) (a) Ojima, L.; McCarthy, J. R.; Welch, J. T. *Biomedical Frontiers of Fluorine Chemistry*; American Chemical Society: Washington, D.C., 1996. (b) Hudlicky, M. In *Chemistry of Organic Fluorine Compounds*, 2nd ed.; Horwood, E., Mellor, J., Eds.; Ellis Horwood and PTR Prentice Hall: New York, 1992. (c) Welch, J. T. *Tetrahedron* **1987**, *43*, 3123. (d) Wilkinson, J. A. *Chem. Rev.* **1992**, *92*, 505.
(4) (a) Gelb, M. H.; Svaren, J. P.; Abeles, R. H. *Biochemistry* **1985**, *24*, 1813. (b) Angliker, H.; Wikstrom, P.; Rauber, P.; Stone, S.; Shaw, E. *Biochem. J.* **1988**, *256*, 481. (c) Abdel-Aal, Y. A. I.; Hammock, B. D. *Insect Biochem.* **1985**, *15*, 111. (d) Ashour, M.-B. A.; Hammock, B. D. *Biochem. Pharmacol.* **1987**, *36*, 1869. (e) Street, I. P.; Lin, H. K.; Laliberté, F.; Ghomashchi, F.; Wang, Z.; Perrier, H.; Tremblay, N. M.; Huang, Z.; Weech, P. K.; Gelb, M. H. *Biochemistry* **1993**, *32*, 5935.
(5) Koutek, B.; Prestwich, G. D.; Howlett, A. C.; Chin, S. A.; Salehani, D.; Akhavan, N.; Deutsch, D. G. *J. Biol. Chem.* **1994**, *269*, 22937.
(6) Patel, D. V.; Rielly-Gauvin, K.; Ryono, D. E. *Tetrahedron. Lett.* **1988**, *29*, 4665.
(7) (a) Durán, I.; Parrilla, A.; Feixas, J.; Guerrero, A. *Bioorg. Med. Chem. Lett.* **1993**, *3*, 2593. (b) Parrilla, A.; Guerrero, A. *Chem. Senses* **1994**, *19*, 1. (c) Parrilla, A.; Villuendas, I.; Guerrero, A. *Bioorg. Med. Chem.* **1994**, *2*, 243. (d) Renou, M.; Lucas, P.; Malo, E.; Quero, C.; Guerrero, A. *Chem. Senses* **1997**, *22*, 407. (e) Bau, J.; Martínez, D.; Renou, M.; Guerrero, A. *Chem. Senses* **1999**, *24*, 473. (f) Riba, M.; Sans, A.; Bau, P.; Grolleau, G.; Renou, M.; Guerrero, A. *J. Chem. Ecol.* **2001**, *27*, 1879.
(8) Quero, C.; Rosell, G.; Jiménez, O.; Rodriguez, S.; Bosch, M. P.; Guerrero, A. *Bioorg. Med. Chem.* **2003**, *11*, 1047.

10.1021/ja043522d CCC: $30.25

Scheme 1

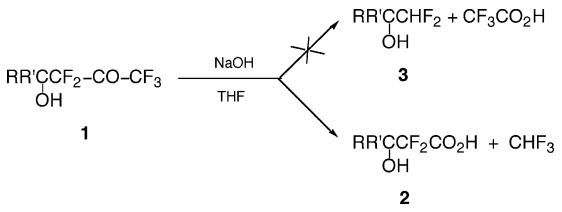

been prepared and tested as inhibitors of the enzymes responsible for the catabolism of the pheromone. It has been noticed that the potency of the inhibitors is higher when an increasing number of the halogen atoms in the carbonyl vicinity is present.[3b,8] In the course of a study aimed at the synthesis of new difluoroalkyl trifluoromethyl ketone analogues of the sex pheromone of the Mediterranean corn borer *Sesamia nonagrioides* an unprecedented haloform-type reaction in which 4-hydroxy-3,3-difluoromethyl trifluoromethyl ketones (**1**) undergo base-promoted cleavage to 3-hydroxy-2,2-difluoroacids (**2**) and fluoroform (CHF_3) in good yields was found (see list of compounds and Table S1, Supporting Information), resulting from the selective cleavage of the CO−CF_3 bond (Scheme 1). On the basis of the expected small bond strength differences between the CO−CF_3 and CO−CF_2R bonds, one would expect the cleavage of **1** to give some trifluoroacetic acid (CF_3CO_2H) and difluoromethyl carbinol (**3**) in addition to the observed formation of **2** and fluoroform. To our surprise, none of the former reaction products were observed in the base-promoted cleavage of **1**.

To rationalize these unexpected results we undertook a theoretical investigation on the mechanism of the hydroxide-ion-initiated cleavage of **1** by means of density functional theory (DFT) calculations. In this investigation we focus on the aforementioned two possible C−C bond cleavage modes of **1**. Since the selective cleavage of **1** to yield **2** and fluoroform turns out to be independent of the nature of substituents R and R′ (see Table S1, Supporting Information), 1,1,1,3,3-pentafluoro-4-hydroxypentan-2-one (**1**, R = CH_3, R′ = H) was chosen to model **1** with an affordable computational cost. To our knowledge, this is the first theoretical study on the mechanism of a haloform-type reaction.

Computational Details

The geometries of the relevant stationary points of the two reaction pathways investigated were optimized using analytical gradient procedures,[9] employing DFT calculations. The Becke three-parameter hybrid functional[10] combined with the Lee, Yang, and Parr (LYP) correlation functional,[11] denoted as B3LYP,[12] was employed with the split-valence 6-311+G(d,p) basis set,[13] which includes d-polarization on carbon and oxygen atoms, p-polarization on the hydrogen atoms, and a single diffuse sp shell[14] on heavy atoms only. All the stationary points were characterized by their harmonic vibrational frequencies as minima or saddle points. Connections of the transition structures between designated minima were confirmed by intrinsic reaction coordinate (IRC)[15] calculations[16] at the B3LYP/6-311+G(d,p) level. All of these calculations were performed with the GAUSSIAN 98 program package.[17]

Zero-point vibrational energies (ZPVEs) were determined from the unscaled harmonic vibrational frequencies calculated at the B3LYP/6-311+G(d,p) level. Thermal corrections to enthalpy, absolute entropies, and Gibbs free-energy values were obtained assuming ideal gas behavior from the unscaled harmonic frequencies and moments of inertia by standard methods.[18] A standard pressure of 1 atm was taken in the absolute entropy calculations.

Basis set superposition error (BSSE) corrections were computed for all complexes located in this study using the counterpoise method.[19,20] The calculated BSSE corrections were found to be small, values ranging from 0.5 to 1.1 kcal/mol.

To investigate the possible solvent-induced changes on the two pathways studied, the solvent effects were introduced within the self-consistent reaction field (SCRF) formalism by means of the polarized continuum model (PCM) of Tomasi et al.[21] as implemented in GAUSSIAN 98. This method models the solvent as a continuum of uniform dielectric and therefore does not take into account explicit solvent−solute interactions such as hydrogen bonding. All PCM calculations were carried out at the B3LYP level of theory with the 6-311+G(d,p) basis set using optimized gas-phase molecular geometries computed at the same level of theory. Two different continuum environments characterized by relative dielectric permittivities of 7.58 (THF) and 78.39 (water) were considered to explore the influence of increasing the dielectric permittivity on the potential-energy barrier of the two reaction pathways investigated.

Results and Discussion

Selected geometrical parameters of the most relevant structures involved in the two reaction pathways studied are shown in Figures 1−3, which are computer-generated plots of the optimized geometries. The Cartesian coordinates of all structures reported in this paper are available as Supporting Information. Total energies calculated in the gas phase as well as the ZPVEs, thermal corrections to enthalpy, and absolute entropies are collected in Table S2 (Supporting Information). Total energies computed in THF and water are given in Table S3 (Supporting Information). For all stationary points and possible reaction products of the two reaction pathways investigated, Tables 1 and 2 give the relative energies (ΔU), the relative energies at 0 K (ΔE(0 K)), the relative enthalpies at 298 K (ΔH(298 K)), and the Gibbs free energies at 298 K (ΔG(298 K)). Finally, Tables 3 and 4 compare the relative energies in the gas phase, THF, and water for all stationary points and possible reaction products, respectively.

(9) (a) Schlegel, H. B. *J. Comput. Chem*. **1982**, *3*, 214. (b) Bofill, J. M. *J. Comput. Chem.* **1994**, *15*, 1.
(10) Becke, A. D. *J. Chem. Phys.* **1993**, *98*, 5648.
(11) Lee, C.; Yang, W.; Parr, R. G. *Phys. Rev. B* **1988**, *37*, 785.
(12) Stevens, P. J.; Devlin, F. J.; Chablowski, C. F.; Frisch, M. J. *J. Phys. Chem.* **1994**, *98*, 11623.
(13) Frisch, M. J.; Pople, J. A.; Binkley. J. S. *J. Chem. Phys.* **1984**, *80*, 3265.
(14) Hehre, W. J.; Radom, L.; Schleyer, P. v. R.; Pople, J. A. *Ab Initio Molecular Orbital Theory*; John Wiley: New York, 1986; pp 86−87.
(15) (a) Fukui, K. *Acc. Chem. Res.* **1981**, *14*, 363. (b) Ishida, K.; Morokuma, K.; Kormornicki, A. *J. Chem. Phys.* **1977**, *66*, 2153.
(16) (a) Gonzalez, C.; Schlegel, H. B. *J. Chem. Phys.* **1989**, *90*, 2154. (b) Gonzalez, C.; Schlegel, H. B. *J. Phys. Chem.* **1990**, *94*, 5523.
(17) Frisch, M. J.; Trucks, G. W.; Schlegel, H. B.; Scuseria, M. A.; Robb, M. A.; Cheeseman, J. R.; Zakrzewski, V. G.; Montgomery, J. A.; Stratmann, R. E.; Burant, J. C.; Dapprich, S.; Milliam, J. M.; Daniels, A. D.; Kudin, K. N.; Strain, M. C.; Farkas, O.; Tomasi, J.; Barone, V.; Cossi, M.; Cammi, R.; Mennucci, B.; Pomelli, C.; Adamo, C.; Clifford, S.; Ochterski, J.; Petersson, G. A.; Ayala, P. Y.; Cui, Q.; Morokuma, K.; Malick, D. K.; Rabuck, A. D.; Raghavachari, K.; Foresman, J. B.; Cioslowski, J.; Ortiz, J. V.; Stefanow, B. B.; Liu, G.; Liashenko, A.; Piskorz, P.; Komaromi, A.; Gomperts, R.; Martin, R. L.; Fox, D. J.; Keith, T.; Al-Laham, M. A.; Peng, C. Y.; Nanayakkara, A.; Gonzalez, C.; Challacombe, M.; Gill, P. M. W.; Johnson, B. G.; Chen. W.; Wong, M. W.; Andres, J. L.; Head-Gordon, M.; Replogle, E. S.; Pople, J. A. *GAUSSIAN 98*, Revision A.11; Gaussian, Inc.: Pittsburgh, PA, 1998.
(18) See, e.g.: McQuarrie, D. *Statistical Mechanics;* Harper and Row: New York, 1986.
(19) Boys, S. F.; Bernardi, F. *Mol. Phys.* **1970**, *19*, 553.
(20) van Duijneveldt, F. B.; van Duijneveldt-van de Rijdt, J. G. C. M.; Lenthe, J. H. *Chem. Rev.* **1994**, *94*, 1873.
(21) (a) Miertus, S.; Scrocco, E.; Tomasi, J. *Chem. Phys.* **1981**, *55*, 117. (b) Miertus, S.; Tomasi, J. *Chem. Phys.* **1982**, *65*, 239. (c) Tomasi, J.; Persico, M. *Chem. Rev.* **1994**, *94*, 2027.

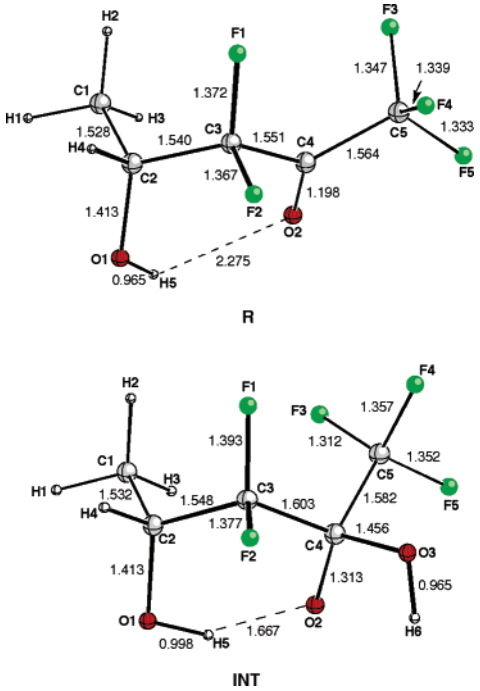

Figure 1. Selected geometrical parameters of the B3LYP/6-311+G(d,p)-optimized geometries of the equilibrium structures for 1,1,1,3,3-pentafluoro-4-hydroxypentan-2-one (**R**) and the anionic tetrahedral intermediate (**INT**). Distances are given in Å.

Reactant. The lowest energy rotational conformer of 1,1,1,3,3-pentafluoro-4-hydroxypentan-2-one, labeled as **R**, is shown in Figure 1. This conformer has the hydroxyl hydrogen atom H5 pointing directly toward the oxygen atom O2 with an H···O distance of 2.275 Å. This geometrical feature indicates that in the gas phase this conformer is energetically stabilized by intramolecular hydrogen bonding. However, it is unlikely that in solution this conformer will be energetically more stable than alternative conformers without internal hydrogen bonds.

Anionic Tetrahedral Intermediate. The attack of hydroxide ion on the carbonyl of **R** leads to the formation of an anionic tetrahedral intermediate. Numerous attempts to locate a transition structure for this process were unsuccessful. On the basis of the expected high electrophilicity of the carbonyl carbon atom caused by the adjacent CF_3 and CF_2 groups, it is likely that the nucleophilic addition of hydroxide ion to the carbonyl of **R** takes place through a barrierless process.

The optimized geometry of the tetrahedral intermediate, labeled as **INT** (Figure 1), was characterized as a local minimum on the potential-energy surface (PES). Compared to **R**, a lengthening of C3−C4 (0.052 Å) and C4−C5 (0.018 Å) is observed for **INT**, reflecting the tendency of these C−C bonds to be broken. The C4−O2 bond is also lengthened (by 0.115 Å), but it is shorter than the C−O bond of a simple alkoxide (i.e., 1.335 Å for methoxide at the same level of theory). As noted for **R**, the O2 and H5 atoms show an intramolecular hydrogen-bonding interaction in **INT**. The distance between these atoms in **INT** (1.667 Å) is substantially shorter than that calculated for **R** (2.275 Å), which indicates that the O2···H5 hydrogen bond in **INT** is much stronger than that in **R**. This

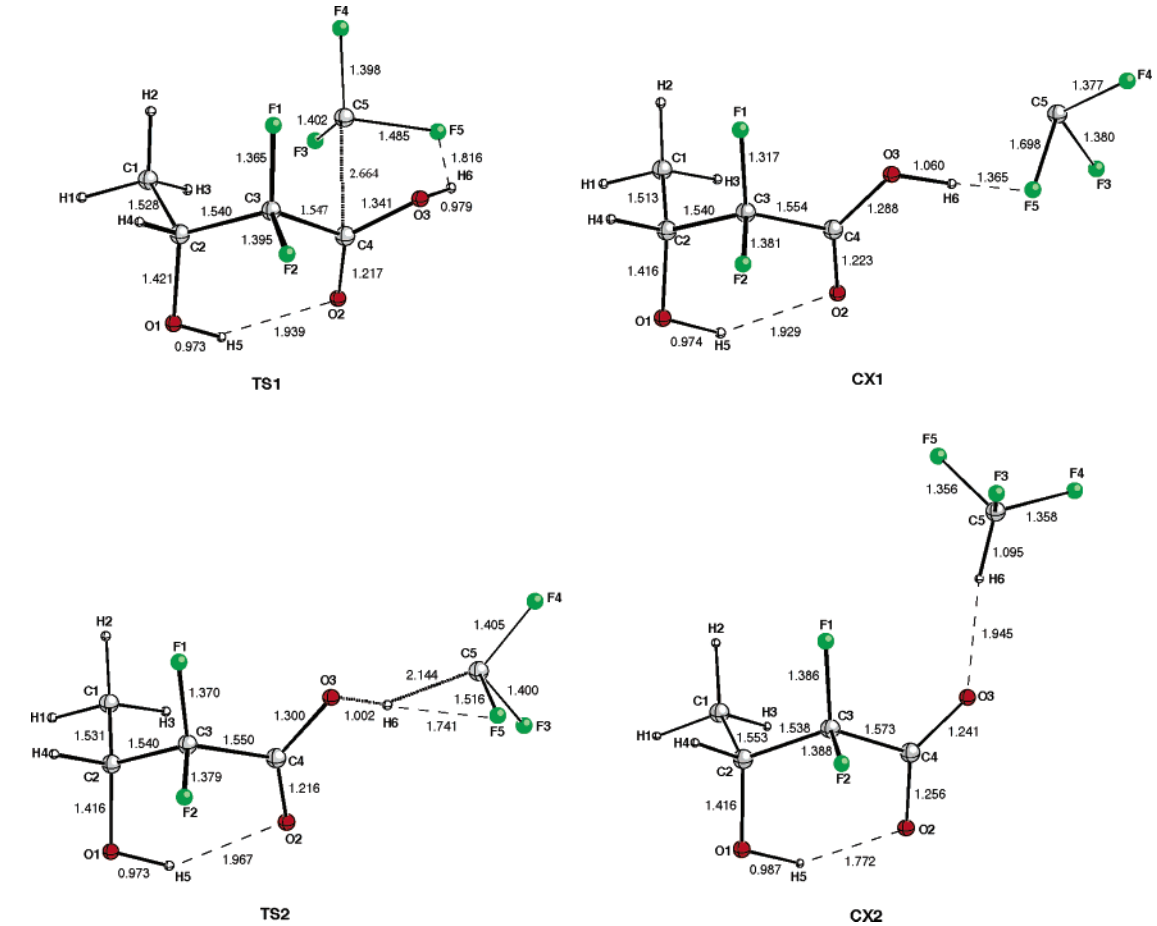

Figure 2. Selected geometrical parameters of the B3LYP/6-311+G(d,p)-optimized geometries of the stationary points on the reaction pathway for the CO−CF_3 bond cleavage in the anionic tetrahedral intermediate. Distances are given in Å.

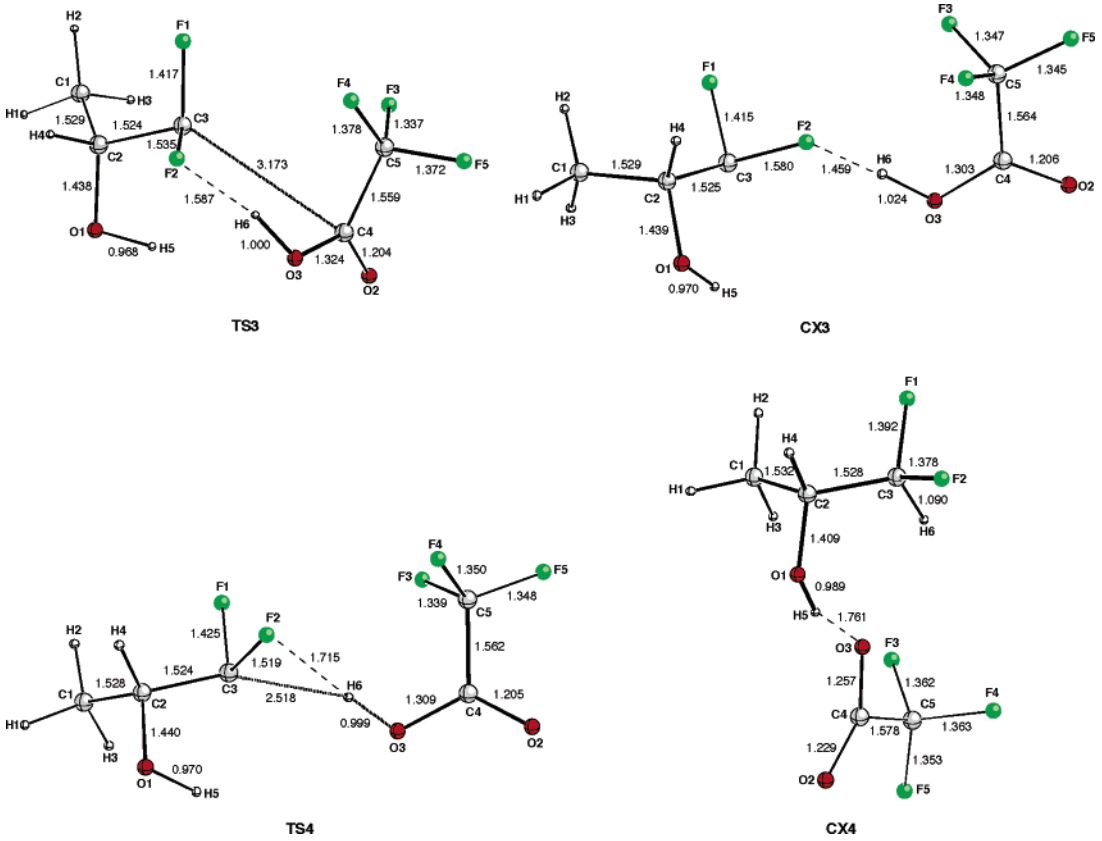

Figure 3. Selected geometrical parameters of the B3LYP/6-311+G(d,p)-optimized geometries of the stationary points on the reaction pathway for the CO−CF_2 bond cleavage in the anionic tetrahedral intermediate. Distances are given in Å.

Table 1. Relative Energies (kcal/mol) of the Stationary Points Involved in the Hydroxide-Ion-Initiated C−C Bond Cleavages of 1,1,1,3,3-Pentafluoro-4-hydroxypentan-2-one (R) in the Gas Phase[a]

structure	ΔU	ΔE (0 K)	ΔH (298 K)	ΔG (298 K)
R + HO^-	74.9	71.6	73.2	61.4
INT	0.0	0.0	0.0	0.0
TS1	23.9	22.1	22.5	20.8
CX1	17.6	14.6	16.0	9.8
TS2	18.7	16.5	17.3	12.9
CX2	−29.0	−29.1	−28.2	−33.5
TS3	33.2	30.9	31.4	29.2
CX3	32.5	29.8	31.1	25.1
TS4	32.7	30.0	30.9	26.4
CX4	−31.4	−31.4	−30.4	−37.1

[a] Calculated at the B3LYP/6-311+G(d,p) level of theory including the BSSE correction.

Table 2. Relative Energies (kcal/mol) of Possible Reaction Products of the Hydroxide-Ion-Initiated C−C Bond Cleavages of 1,1,1,3,3-Pentafluoro-4-hydroxypentan-2-one in the Gas Phase[a,b]

products	ΔU	ΔE (0 K)	ΔH (298 K)	ΔG (298 K)
$CH_3CHOHCF_2CO_2H + CF_3^-$	40.5	38.2	38.9	25.0
$CH_3CHOHCF_2CO_2^- + CHF_3$	−16.5	−17.0	−16.8	−29.6
$CH_3CHOHCF_2^- + CF_3CO_2H$	54.2	51.5	52.2	37.3
$CH_3CHOHCHF_2 + CF_3CO_2^-$	−11.9	−12.9	−12.4	−27.6

[a] Calculated at the B3LYP/6-311+G(d,p) level of theory. [b] The energies are referred to the energy of the reaction intermediate **INT**.

remarkable feature is attributed to the fact that in the anionic intermediate **INT** atom O2 is bearing most of the negative charge. However, as in the case of **R**, it is unlikely that in solution this structure will be energetically more stable than alternative conformers without internal hydrogen bonds.

Table 3. Comparison between the Relative Energies (kcal/mol) in the Gas Phase, THF, and Water of the Stationary Points Involved in the Hydroxide-Ion-Initiated C−C Bond Cleavages of 1,1,1,3,3-Pentafluoro-4-hydroxypentan-2-one (R)[a]

structure	gas phase	THF	water
R + HO^-	74.9	35.1	19.7
INT	0.0	0.0	0.0
TS1	23.9	26.7	26.8
CX1	16.6	18.8	nc[b]
TS2	18.7	18.9	19.3
CX2	−29.5	−27.7	−23.2
TS3	33.2	37.7	40.3
CX3	31.4	36.3	39.1
TS4	32.7	37.5	38.8
CX4	−32.1	−28.5	−10.4

[a] Calculated with the PCM method at the B3LYP level of theory with the 6-311+G(d,p) basis set using the geometries optimized in the gas phase at the same level. [b] The calculation does not converge.

As expected, the nucleophilic addition of hydroxide ion to **R** yielding **INT** is quite exoergic. From the ΔU data given in Table 1 an energy of reaction (ΔU_r) of −74.9 kcal/mol is predicted for this addition. Such exoergicity is substantially larger than that ($\Delta U_r = -35.2$ kcal/mol) calculated by Madura and Jorgensen[22] at the Hartree−Fock (HF) level of theory with the 6-31+G(d) basis set for the addition of hydroxide ion to formaldehyde in the gas phase. The larger exoergicity calculated for the addition of hydroxide ion to **R**, as compared to its addition to formaldehyde, can be traced to the expected higher electrophilicity of the carbonyl carbon in **R** caused by the adjacent CF_3 and CF_2 groups.

(22) Madura, J. D.; Jorgensen, W. L. *J. Am. Chem. Soc.* **1986**, *108*, 2517.

Table 4. Comparison between the Relative Energies (kcal/mol) in the Gas Phase, THF, and Water of Possible Reaction Products of the Hydroxide-Ion-Initiated C−C Bond Cleavages of 1,1,1,3,3-Pentafluoro-4-hydroxypentan-2-one[a,b]

structure	gas phase	THF	water
$CH_3CHOHCF_2CO_2H + CF_3^-$	40.5	24.5	17.9
$CH_3CHOHCF_2CO_2^- + CHF_3$	−16.5	−22.4	−21.5
$CH_3CHOHCF_2^- + CF_3CO_2H$	54.2	54.2	54.2
$CH_3CHOHCHF_2 + CF_3CO_2^-$	−11.9	−11.9	−11.9

[a] Calculated with the PCM method at the B3LYP level of theory with the 6-311+G(d,p) basis set using the geometries optimized in the gas phase at the same level. [b] The energies are referred to the energy of the reaction intermediate **INT**.

Reaction Pathway for the CO−CF_3 Bond Cleavage of the Anionic Tetrahedral Intermediate. The computation of the minimum energy reaction path (MERP) for the CO−CF_3 bond cleavage in **INT** was attempted by simple elongation of the C4−C5 bond. Starting at the equilibrium structure **INT**, the C4−C5 distance was taken as the reaction coordinate, the energy being minimized with respect to all geometrical variables without imposing any geometrical restriction. The increase of the C4−C5 distance caused a simultaneous decrease of the distance between atoms F5 and H6, so the fluorine atom was moving to the hydrogen atom along the reaction pathway. This MERP led eventually to the location of an energy maximum, and this was optimized to the transition structure labeled as **TS1** in Figure 2. In addition to the C4−C5 bond breaking and the persistence of the O2···H5 hydrogen bond, the most remarkable geometrical changes observed in going from **INT** to **TS1** are the shortening of the distance between the F5 and H6 atoms and the lengthening of the C5−F5 and O3−H6 bonds, which are indicative of a hydrogen-bonding interaction between atoms F5 and H6 in **TS1**. From the ΔU data given in Table 1, an energy barrier ($\Delta U^{\ddagger}$) of 23.9 kcal/mol is predicted for the CO−CF_3 bond cleavage of **INT**.

The IRC was followed from **TS1**. The reverse pathway eventually ended back at the tetrahedral intermediate **INT**. The forward pathway ended in a $[CH_3CHOHCF_2CO_2H\cdots CF_3]^-$ complex. The optimized geometry of this complex, labeled as **CX1** (Figure 2), was characterized as a true local minimum on the PES. The most prominent geometrical features of complex **CX1** are the long C5−F5 bond length (1.698 Å) and the short distance between F5 and H6 (1.365 Å), which are indicative of a strong intermolecular hydrogen bond between the latter atom pair. Therefore, **CX1** turns out to be a hydrogen-bonded complex. At this point it is worth noting that **CX1** lies 22.9 kcal/mol below the energy of the isolated components $CH_3CHOHCF_2CO_2H$ and CF_3^- (see the ΔU data in Tables 1 and 2). This result can be easily rationalized in terms of the aforementioned strong F5···H6 hydrogen bond and the attractions between charges and ion−dipole and higher moments, ion-induced dipole interactions, and dispersion forces holding in association the two components of **CX1**.[23]

The second step of the C4−C5 bond cleavage in **INT** was found to be a proton transfer between the $CH_3CHOHCF_2CO_2H$ and CF_3^- components in the hydrogen-bonded complex **CX1**. The optimized geometry of the transition structure for this proton transfer, labeled as **TS2**, is shown in Figure 2. The geometrical changes observed in passing from **CX1** to **TS2** suggest that this transition structure involves the concerted making of a covalent bond between atoms C5 and H6, the breaking of the covalent bond O3−H6, and the breaking of the hydrogen bond between the atoms F5 and H6. The ΔU data listed in Table 1 show that this process involves a $\Delta U^{\ddagger}$ of only 1.1 kcal/mol.

The IRC calculations showed that **TS2** goes backward to the complex **CX1** and goes forward to give a $[CH_3CHOHCF_2CO_2\cdots CHF_3]^-$ complex. The optimized geometry of this complex, labeled as **CX2** (Figure 2), was characterized as a true local minimum on the PES. The distance of 1.945 Å between atoms O3 and H6 is indicative of intermolecular hydrogen bonding in **CX2**. Thus, it appears that **CX2** is a hydrogen-bonded complex. The ΔU data listed in Table 1 show that the proton transfer in **CX1** leading to **CX2** is a highly exoergic process involving a ΔU_r of −46.6 kcal/mol. This result can be easily rationalized in terms of the expected larger gas-phase pK_a value of $CH_3CHOHCF_2CO_2H$ compared to that of CHF_3. Interestingly, complex **CX2** lies 12.5 kcal/mol below the energy of the isolated components $CH_3CHOHCF_2CO_2^-$ and CHF_3 (see the ΔU data in Tables 1 and 2). Such stabilization energy with respect to these isolated products arises from the O3···H6 hydrogen bonding and the attractions between charges and ion−dipole and higher moments, ion-induced dipole interactions, and dispersion forces holding in association the two components of this complex. We did not find an energy barrier other than that imposed by the endoergicity for the **CX2** complex to break apart to form the isolated products $CH_3CHOHCF_2CO_2^-$ and CHF_3.

To summarize the thermodynamics of the overall reaction pathway for the gas-phase addition of hydroxide ion to **R** leading to CO−CF_3 bond cleavage, the calculated ΔG(298 K) of the stationary points relative to the Gibbs free energy at 298 K of intermediate **INT** are displayed in Figure 4. Starting from isolated **R** and hydroxide ion, the tetrahedral intermediate **INT** is barrierless, formed with a Gibbs free energy of reaction at 298 K (ΔG_r(298 K)) of −61.4 kcal/mol. This intermediate undergoes CO−CF_3 bond cleavage to the hydrogen-bonded complex **CX1** by passage through transition structure **TS1**. This process has associated with it a Gibbs free energy of activation at 298 K ($\Delta G^{\ddagger}$(298 K)) of 20.8 kcal/mol and a ΔG_r (298 K) of 9.8 kcal/mol. The complex **CX1** then experiences a proton transfer between its components, yielding the hydrogen-bonded complex **CX2**. This process takes place through the transition structure **TS2** and involves a $\Delta G^{\ddagger}$(298 K) of only 3.1 kcal/mol and a ΔG_r(298 K) of −43.3 kcal/mol. Finally, the hydrogen-bonded complex **CX2** can break apart to form the fully dissociated $CH_3CHOHCF_2CO_2^-$ and CHF_3 reaction products with a ΔG(298 K) of 3.9 kcal/mol.

At this point we note that the overall reaction pathway for the gas-phase addition of hydroxide ion to **R** yielding $CH_3CHOHCF_2CO_2^-$ and CHF_3 is a highly exoergic process involving a ΔG_r(298 K) of −91.0 kcal/mol. The rate-determining step of the overall reaction pathway is the CO−CF_3 bond cleavage in **INT** leading to **CX1** through **TS1** with a $\Delta G^{\ddagger}$(298 K) of 20.8 kcal/mol. Since the addition of hydroxide ion to **R** yielding **INT** is highly exoergic (ΔG_r(298 K) = −61.4 kcal/mol), it follows that when formed from these reactants **INT**

(23) (a) Morton, T. H. *Tetrahedron* **1982**, *38*, 3195. (b) McAdoo, D. J. *Mass Spectrom. Rev.* **1988**, *7*, 363. (c) Bouchoux, G. *Adv. Mass Spectrom.* **1989**, *11*, 812. (d) Hammerum, S. In *Fundamentals of Gas-Phase Ion Chemistry*; Jennings, K. R., Ed.; Kluwer Academic Publishers: Dordrecht, The Netherlands, 1990; pp 379−390. (e) Bowen, R. D. *Acc. Chem. Res.* **1991**, *24*, 364. (f) Longevialle, P. *Mass Spectrom. Rev.* **1992**, *11*, 157. (g) McAdoo, D. J.; Morton, T. H. *Acc. Chem. Res.* **1993**, *26*, 295.

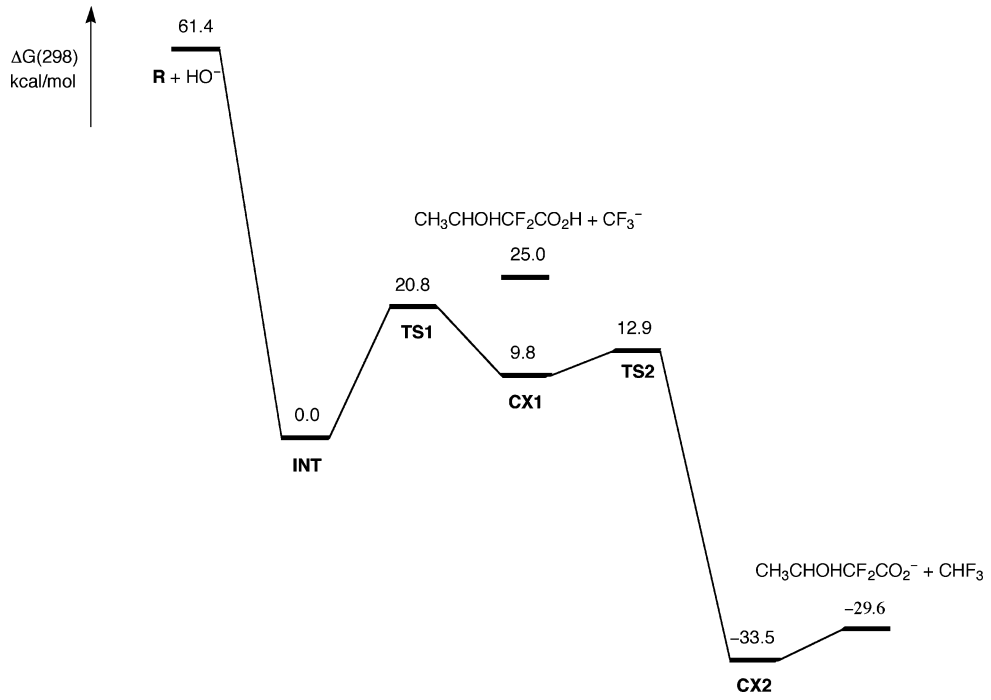

Figure 4. Reaction pathway for hydroxide-ion-initiated CO−CF_3 bond cleavage in 1,1,1,3,3-pentafluoro-4-hydroxypentan-2-one (**R**). Gibbs free energies at 298 K of stationary points are graphed relative to Gibbs free energy at 298 K of the tetrahedral intermediate (**INT**).

contains an excess of energy, which is stored in vibrations and rotations. It is likely, therefore, that such energy excess suffices for overcoming the $\Delta G^{\ddagger}$(298 K) of 20.8 kcal/mol.

Reaction Pathway for the CO−CF_2 Bond Cleavage of the Anionic Tetrahedral Intermediate. Computation of the MERP for the CO−CF_2 bond cleavage in **INT** was attempted by simple elongation of the C3−C4 bond. Starting at the equilibrium structure **INT**, the C3−C4 distance was taken as the reaction coordinate, the energy being minimized with respect to all geometrical variables without imposing any geometrical restriction. The increase of the C3−C4 distance caused a simultaneous decrease of the distance between atoms F2 and H6, so the fluorine atom was moving to the hydrogen atom along the reaction pathway. This MERP led eventually to the location of an energy maximum, and this was optimized to the transition structure labeled as **TS3** in Figure 3. In addition to the C3−C4 bond breaking and the disappearance of the O2···H5 hydrogen bond, the most remarkable geometrical changes observed in going from **INT** to **TS3** are the shortening of the distance between the F2 and H6 atoms and the lengthening of the C5−F5 and O3−H6 bonds, which are indicative of a hydrogen-bonding interaction between atoms F2 and H6 in **TS3**. Compared to **TS1**, the C−C bond being broken is 0.509 Å longer in **TS3** and the former O2···H5 hydrogen bond in **INT** is lacking in **TS3**.

The IRC calculations showed that **TS3** goes backward to the tetrahedral intermediate **INT** and goes forward to give a $[CH_3CHOHCF_2\cdots CF_3CO_2H]^-$ complex. The optimized geometry of this complex, labeled as **CX3** (Figure 3), was characterized as a true local minimum on the PES. The most remarkable geometrical features of complex **CX3** are the long C3−F2 bond length (1.580 Å) and the short F2···H6 distance (1.459 Å), which are indicative of a strong intermolecular hydrogen bond between the latter atom pair. Therefore, **CX3** turns out to be a hydrogen-bonded complex. From the energy point of view, it is important to note that **CX3** is predicted to lie 14.9 kcal/mol above the energy of **CX1** (see the ΔU data in Table 1). In addition, the energy of the isolated components of **CX3**, namely, $CH_3CHOHCF_2^-$ and CF_3CO_2H, is predicted to be 13.7 kcal/mol higher than the energies of the isolated components of **CX1**, namely, $CH_3CHOHCF_2CO_2H$ and CF_3^- (see the ΔU data in Table 2). These predictions are easily understood on the basis of the high electronegativity of fluorine. In fact, the negative charge is energetically more stabilized in CF_3^- than in $CH_3CHOHCF_2^-$ because of the larger number of fluorine atoms bonded to the carbon atom bearing the negative charge. On the other hand, it is worthwhile to note that the stabilization energy of **CX3** with respect to its isolated components, namely, 21.7 kcal/mol (see the ΔU data in Tables 1 and 2), is similar to that (22.9 kcal/mol) mentioned above for complex **CX1** with respect to the corresponding isolated components.

From the ΔU data given in Table 1, a $\Delta U^{\ddagger}$ of 33.2 kcal/mol is predicted for the CO−CF_2 bond cleavage in **INT**, which is 9.3 kcal/mol higher than that (23.9 kcal/mol) found for the CO−CF_3 bond cleavage. In keeping with the higher energy of **CX3** compared to **CX1**, this result is ascribed to the high electronegativity of fluorine. Specifically, the fluorine atoms inside the moieties of **TS1** and **TS3**, which become later the anionic components of the **CX1** and **CX3** complexes (i.e., CF_3 and $CH_3CHOHCF_2$), stabilize the negative charge accumulated on these moieties. As expected, the energy stabilization arising from this effect is larger for **TS1** than for **TS3** because of the larger number of fluorine atoms in the aforementioned moiety of **TS1**.

The second step of the C3−C4 bond cleavage in **INT** was found to be a proton transfer between the $CH_3CHOHCF_2^-$ and CF_3CO_2H components in the hydrogen-bonded complex **CX3**. The optimized geometry of the transition structure for this proton transfer, labeled as **TS4**, is shown in Figure 3. The geometrical changes observed in passing from **CX3** to **TS4** suggest that this transition structure involves the concerted making of a covalent

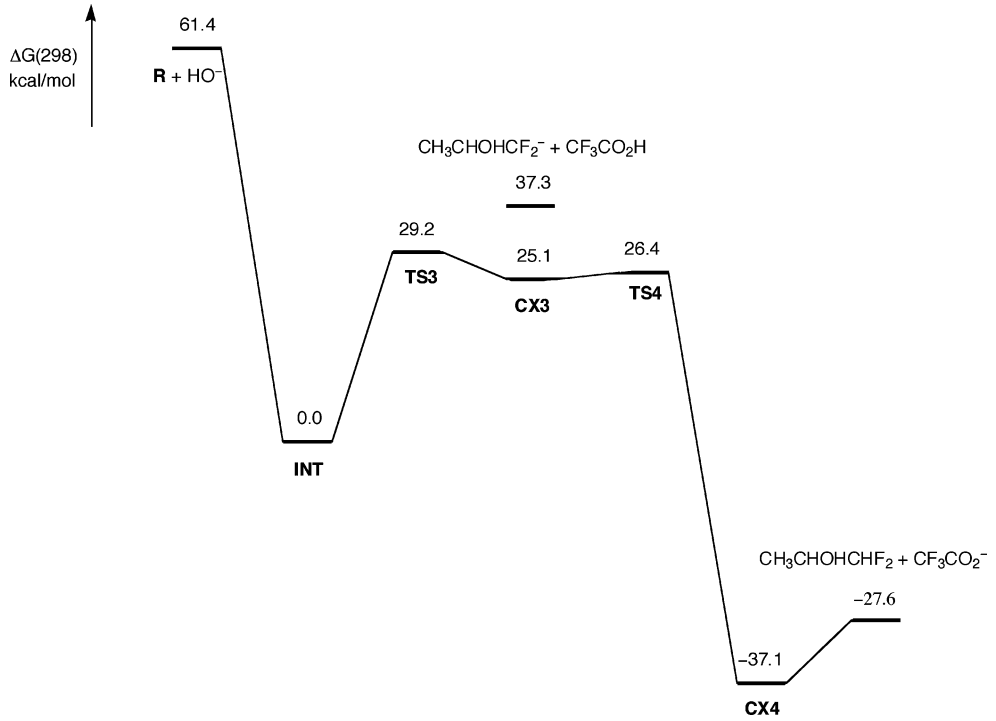

Figure 5. Reaction pathway for hydroxide-ion-initiated CO−CF_2 bond cleavage in 1,1,1,3,3-pentafluoro-4-hydroxypentan-2-one (**R**). Gibbs free energies at 298 K of stationary points are graphed relative to Gibbs free energy at 298 K of the tetrahedral intermediate (**INT**).

bond between atoms C3 and H6, the breaking of the covalent bond O3−H6, and the breaking of the hydrogen bond between atoms F2 and H6. The ΔU data listed in Table 1 show that this proton-transfer step involves a $\Delta U^{\ddagger}$ of only 0.2 kcal/mol.

The IRC calculations showed that **TS4** goes backward to complex **CX3** and goes forward to give a $[CH_3CHOHCHF_2\cdots CF_3CO_2]^-$ complex. The optimized geometry of this complex, labeled as **CX4** (Figure 3), was characterized as a true local minimum on the PES. The short distance of 1.761 Å between atoms O3 and H5 is indicative of an intermolecular hydrogen bonding in **CX4**. Thus, it appears that **CX4** is a hydrogen-bonded complex. The ΔU data listed in Table 1 shows that the proton transfer in **CX3** leading to **CX4** is a highly exoergic process involving a ΔU_r of −63.9 kcal/mol. This result can be easily rationalized in terms of the expected larger gas-phase pK_a value of CF_3CO_2H compared to that of $CH_3CHOHCHF_2$. Complex **CX4** lies 19.5 kcal/mol below the energy of its isolated components $CH_3CHOHCHF_2$ and $CF_3CO_2^-$ (see the ΔU data in Tables 1 and 2). Interestingly, this stabilization energy of **CX4** is 7.0 kcal/mol larger than that (12.5 kcal/mol) calculated for the stabilization energy of **CX2** with respect to the corresponding isolated components. This result can be attributed to the expected lower stabilization energy associated with the C4−O3···H6−C5 hydrogen-bonding interaction in **CX2** as compared to the O1−H5···O3−C4 hydrogen-bonding interaction for the **CX4** case. As for complex **CX2**, we did not find an energy barrier other than that imposed by the endoergicity for the **CX4** complex to break into its isolated components.

Figure 5 summarizes the thermodynamics of the overall reaction pathway for the gas-phase addition of hydroxide ion to **R**, leading to CO−CF_2 bond cleavage. As found for the CO−CF_3 bond cleavage, the reaction pathway starts with formation of the anionic tetrahedral intermediate **INT**. This intermediate then undergoes CO−CF_2 bond cleavage to the hydrogen-bonded complex **CX3** by passage through transition structure **TS3**. This process involves a $\Delta G^{\ddagger}$(298 K) of 29.2 kcal/mol and a ΔG_r(298 K) of 25.1 kcal/mol. The complex **CX3** experiences a proton transfer between its components, giving the hydrogen-bonded complex **CX4**. This process takes place through transition structure **TS4** and involves a $\Delta G^{\ddagger}$(298 K) of only 1.3 kcal/mol and a ΔG_r(298 K) of −62.2 kcal/mol. Finally, the hydrogen-bonded complex **CX4** can break apart to form the fully dissociated $CH_3CHOHCHF_2$ and $CF_3CO_2^-$ reaction products with a ΔG(298 K) of 9.5 kcal/mol.

The overall reaction pathway for the gas-phase addition of hydroxide ion to **R** yielding $CH_3CHOHCHF_2$ and $CF_3CO_2^-$ is a highly exoergic process involving a ΔG_r(298 K) of −89.0 kcal/mol. The rate-determining step of the overall reaction pathway is the CO−CF_2 bond cleavage in **INT** leading to **CX3** through **TS3**. This process involves a $\Delta G^{\ddagger}$(298 K) of 29.2 kcal/mol, which is 8.4 kcal/mol higher than that found for the alternative CO−CF_3 bond cleavage in **INT** leading to **CX1** through **TS1**. It follows, therefore, that the hydroxide-ion-promoted cleavage of the CO−CF_3 bond of **R** yielding $CH_3CHOHCF_2CO_2^-$ and CHF_3 is clearly favored over the cleavage of the CO−CF_2 bond leading to $CH_3CHOHCHF_2$ and $CF_3CO_2^-$.

Solvent Effects. Table 3 shows that solvation increases the energy of all the complexes found on the two reaction pathways investigated, while Table 4 shows that the solvent lowers the energy of the corresponding isolated components. It turns out, therefore, that solvation substantially decreases the stabilization energy of the complexes with respect to their isolated components.

The most significant effect of solvation on the other stationary points located on the two reaction pathways (Table 3) is to lower the energy of the isolated reactants hydroxide ion and **R** with respect to the tetrahedral intermediate **INT** by 39.8 (THF) or

55.2 kcal/mol (water). As a consequence, when formed from these reactants **INT** contains a lower excess of energy in solution than in the gas phase. On the other hand, solvation increases the energy of **TS1** by 2.8 (THF) or 2.9 kcal/mol (water) and that of **TS3** by 4.5 (THF) or 7.1 kcal/mol (water) with respect to the energy of **INT**. Thus, the solvent effects do not reverse the preference found for the CO−CF_3 over the CO−CF_2 bond cleavage in **INT** in the gas phase. On the contrary, the hydroxide-ion-promoted cleavage of the CO−CF_3 bond of **R** is predicted to be even more favored over CO−CF_2 bond cleavage in solution than in the gas phase. Nevertheless, the increase in the energy of **TS1** relative to that of **INT**, caused by solvation, combined with the decrease in the excess of energy contained in **INT**, when formed in solution, indicates that the hydroxide-ion-promoted cleavage of **R** should be slower in solution than in the gas phase.

Summary and Conclusions

In an attempt to rationalize the recent experimental results of an unprecedented haloform-type reaction in which 4-alkyl-4-hydroxy-3,3-difluoromethyl trifluoromethyl ketones undergo base-promoted cleavage to 3-hydroxy-2,2-difluoroacids and fluoroform in good yields, resulting from selective cleavage of the CO−CF_3 bond, we investigated by means of DFT calculations with the B3LYP functional the two possible C−C bond cleavage modes of 1,1,1,3,3-pentafluoro-4-hydroxypentan-2-one (**R**) in the gas phase. In addition, we also investigated the possible solvent-induced changes on the two pathways using the PCM method. From the analysis of the results of the B3LYP calculations, the following main points emerge.

(1) The gas-phase addition of hydroxide ion to the carbonyl carbon atom of **R** leads to the barrierless formation of an anionic tetrahedral intermediate, **INT,** with a ΔG_r(298 K) of −61.4 kcal/mol.

(2) The CO−CF_3 bond cleavage of **INT** in the gas phase leads to the formation of a hydrogen-bonded [$CH_3CHOHCF_2CO_2H\cdots CF_3$]$^-$ complex, **CX1**, by passage through a transition structure **TS1** with a $\Delta G^{\ddagger}$(298 K) of 20.8 kcal/mol. **CX1** undergoes a proton transfer between its components yielding a hydrogen-bonded [$CH_3CHOHCF_2CO_2\cdots CHF_3$]$^-$ complex, **CX2**, with a $\Delta G^{\ddagger}$(298 K) of only 3.1 kcal/mol. Finally, complex **CX2** can break apart to form the fully dissociated components with a ΔG(298 K) of 3.9 kcal/mol.

(3) The CO−CF_2 bond cleavage of **INT** in the gas phase leads to the formation of a hydrogen-bonded [$CH_3CHOHCF_2\cdots CF_3CO_2H$]$^-$ complex, **CX3**, by passage through a transition structure **TS3** with a $\Delta G^{\ddagger}$(298 K) of 29.2 kcal/mol, which is 8.4 kcal/mol higher than that found for the alternative CO−CF_3 bond cleavage. In keeping with the higher energy found for **CX3**, as compared to **CX1**, the higher energy of **TS3** is due chiefly to the smaller number of fluorine atoms stabilizing the negative charge accumulated on the $CH_3CHOHCF_2$ moiety of **TS3**, as compared to the larger number of fluorine atoms stabilizing the negative charge on the CF_3 moiety of **TS1**.

(4) The solvent-induced effects on the two pathways do not reverse the predicted preference for the CO−CF_3 over the CO−CF_2 bond cleavage of **INT** in the gas phase. On the contrary, the hydroxide-ion-promoted cleavage of the CO−CF_3 bond of **R** is predicted to be even more favored over CO−CF_2 bond cleavage in solution than in the gas phase.

In accord with experimental findings, the above points suggest that the hydroxide-ion-promoted cleavage of the CO−CF_3 bond of **R**, yielding $CH_3CHOHCF_2CO_2^-$ and CHF_3, is clearly favored over cleavage of the CO−CF_2 bond leading to $CH_3CHOHCHF_2$ and $CF_3CO_2^-$.

Acknowledgment. This research was supported by the Spanish DGICYT (Grants BQU2002-04485-C02-01, BQU2002-04485-C02-02, and AGL2003-06599-C02-01). Additional support came from Catalonian CIRIT (Grant 2001SGR00048). The larger calculations described in this work were performed on the CPQ AlphaServer HPC320 at the Centre de Supercomputació de Catalunya (CESCA).

Supporting Information Available: List of compounds and table containing examples of the base-promoted cleavage of 4-alkyl-4-hydroxy-3,3-difluoromethyl trifluoromethyl ketones, the Cartesian coordinates of all structures reported in this paper, and tables summarizing total energies, zero-point vibrational energies, thermal corrections to enthalpy, and absolute entropies. This material is available free of charge via the Internet at http://pubs.acs.org.

JA043522D